Tableau 6. *Distances interatomiques intermoléculaires* (Å) *inférieures à* 3,80 Å *et écarts types*

C(1)–O^{i}	3,456 (4)	C(3)–N^{ii}	3,737 (3)
C(1)–C(6^{i})	3,687 (5)	C(4)–O^{i}	3,624 (4)
C(2)–O^{i}	3,666 (4)	C(4)–C(9^{iii})	3,631 (5)
C(2)–C(4^{ii})	3,666 (4)	C(4)–N^{ii}	3,657 (4)
C(2)–C(3^{ii})	3,672 (4)	C(8)–C(10^{iv})	3,715 (4)
C(3)–O^{ii}	3,696 (3)	O–N^{ii}	2,860 (3)

Code de symétrie

(i)	$y-1, x, 1-z$	(iii)	$x, y-1, z$
(ii)	$y, x, 1-z$	(iv)	$\frac{1}{2}-x, \frac{1}{2}+y, \frac{3}{4}+z$

cote z forment des couches parallèles au plan (001). Les noyaux phényle sont disposés de part et d'autre de ces couches de façon que les plans des noyaux phényle appartenant à deux couches adjacentes soient perpendiculaires entre eux.

La Fig. 2 montre une vue stéréoscopique de l'enchaînement moléculaire. Le cohésion cristalline est assurée par des interactions de van der Waals. Les distances interatomiques intermoléculaires inférieures à 3,80 Å sont portées dans le Tableau 6.

Conclusion

La structure cristalline de la (−)-(*S*)-*N*-(phényl-1 éthyl)-acétamide ne fait pas apparaître d'interactions définies autres que la formation d'une liaison hydrogène intermoléculaire. En particulier, la disposition approximativement orthogonale des cycles phényle des molécules voisines exclut tout effet de 'stacking'.

Il semble donc au vu de ces résultats que le phénomène de dédoublement spontané de la *N*-(phényl-1 éthyl)-acétamide soit principalement dû à des raisons d'empilement moléculaire optimal lors de la formation du cristal. On peut signaler à l'appui de cette hypothèse que le composé homologue dans lequel le groupe méthyle $C(1)H_3$ est substitué par un groupement isopropyle ne présente plus de dédoublement spontané des énantiomères par cristallisation (Aubry, Protas, Cung & Marraud, 1980) bien que les molécules liées entre elles par des interactions hydrogène soient de même chiralité.

Références

AUBRY, A., PROTAS, J., CUNG, M. T. & MARRAUD, M. (1980). *Acta Cryst.* B**36**, 96–99.

BUSING, W. R., MARTIN, K. O. & LEVY, H. A. (1962). *ORFLS*. Report ORNL-TM-305. Oak Ridge National Laboratory, Tennessee.

COLLET, A., BRIENNE, M. J. & JACQUES, J. (1972). *Bull. Soc. Chim. Fr.* pp. 127–142.

CUNG, M. T., MARRAUD, M. & NÉEL, J. (1976). *Biopolymers*, **15**, 2081–2095.

GERMAIN, G., MAIN, P. & WOOLFSON, M. M. (1970). *Acta Cryst.* B**26**, 274–285.

GUETTÉ, M. & GETTÉ, J. P. (1977). *Bull. Soc. Chim. Fr.* pp. 769–772.

HARGER, M. J. P. (1977). *J. Chem. Soc. Perkin Trans.* 2, pp. 1882–1887.

JOHNSON, C. K. (1965). *ORTEP*. Report ORNL-3794. Oak Ridge National Laboratory, Tennessee.

KABACHNIK, M. I., MASTRYUKOVA, T. A., FEDIN, E. I., VAISBERG, M. S., MOROZOV, L. L., PETROVSKY, P. V. & SHIPOV, A. E. (1976). *Tetrahedron*, **32**, 1719–1728.

MOREAU, A. & GUETTÉ, J. P. (1974). *Tetrahedron*, **30**, 1923–1931.

NERDEL, F. & LIEBIG, H. (1959). *Justus Liebigs Ann. Chem.* **621**, 42.

PASTEUR, L. (1850). *Ann. Chim. Phys.* **28**, 56–99.

RAMACHANDRAN, G. N., KOLASKAR, A. S., RAMAKRISHNAN, C. & SASISEKHARAN, V. (1974). *Biochim. Biophys. Acta*, **359**, 298–302.

WINKLER, F. K. & DUNITZ, J. D. (1971). *J. Mol. Biol.* **59**, 169–182.

Acta Cryst. (1980). B**36**, 1864–1876

Experimental Electron Density Distributions of Hydrogen Bonds. High-Resolution Study of α-Oxalic Acid Dihydrate at 100 K

BY E. D. STEVENS AND P. COPPENS

Department of Chemistry, State University of New York at Buffalo, Buffalo, New York 14214, *USA*

(*Received* 13 *August* 1979; *accepted* 24 *March* 1980)

Abstract

The electron density of the α form of oxalic acid dihydrate, $C_2H_2O_4.2H_2O$, been determined at 100 K from high-resolution X-ray intensity measurements. Positions of the carbon and oxygen atoms determined by refinement of data with $\sin\theta/\lambda > 1{\cdot}0$ Å^{-1} are in excellent agreement with neutron diffraction values, but

0567-7408/80/081864-13$01.00

thermal parameters are systematically larger. The estimated error in the experimental electron density maps is 0·02 e/Å^3 except near atom centers. A continuous ridge with a saddle point of 0·24 (2) e/Å^3 is observed in the valence density of the short [O···O = 2·487 (1) Å] hydrogen bond between the donor hydrogen atom of oxalic acid and oxygen-atom acceptor on the water molecule. Plots of the deviation from cylindrical symmetry of the covalent-bond peaks reveal significant π character in the C—C, C—O and C=O bonds of the oxalic-acid molecule. Stereographic projection of the non-bonding density on a spherical surface centered on the oxygen atoms reveals a distortion of the lone-pair density on the water oxygen atom in the direction of the short hydrogen bond. The perturbation due to hydrogen bonding is also evident in the out-of-plane displacement of the water molecule dipole moment evaluated from the experimental data. [Crystal data: space group $P2_1/n$, a = 6·0968 (7), b = 3·4975 (4), c = 11·9462 (15) Å, β = 105·78 (1)°, Z = 2, D_x = 1·708 Mg m^{-3}, μ(Mo $K\alpha$) = 0·170 mm^{-1}.]

Introduction

Numerous charge-density studies (for reviews, see Coppens, 1975, 1977; Coppens & Stevens, 1977) have demonstrated that the distortion of atoms as a result of covalent bonding in molecules is observable with accurate X-ray (and neutron) diffraction measurements. In the past decade, improvements in experimental design, methods of data collection and corrections for systematic errors have significantly improved resolution and accuracy of electron density determinations. In addition to the effects of covalent bonding, distortions due to weaker forces such as intermolecular interactions in the solid may now become observable.

One of the strongest and most interesting among intermolecular interactions is hydrogen bonding. Hydrogen bonds vary over a considerable range from an O···O distance of approximately 2·8 Å for a typical 'long' hydrogen bond to about 2·4 Å for a strong hydrogen bond. The electronic structure of hydrogen bonds has been extensively studied by theoretical techniques (Kollman, 1977; Allen, 1975) and, to a lesser extent, by experimental charge density measurements (Olovsson, 1980).

Experimental densities (for example Stevens, 1978; Kvick, Thomas & Koetzle, 1976; Griffin & Coppens, 1975) are in agreement with the theoretical description of long hydrogen bonds as largely electrostatic interactions (Yamabe & Morokuma, 1975; Dreyfus & Pullman, 1970). In contrast, theoretical calculations of short hydrogen bonds show deviations from the electrostatic model (Desmeules & Allen, 1980; Kollman & Allen, 1972), while recent experimental studies (Stevens, Lehmann & Coppens, 1977; Schlemper & Hsu, 1978; Olovsson, Kvick, Lehmann & Olovsson, 1980) suggest a significant covalent contribution.

In solids, a continuous distribution in hydrogen-bond lengths is observed, suggesting that any description of the electronic structure must include a continuous variation from electrostatic to covalent bonding character. However, most studies have concentrated on the two extremes of the long and short bonds, while little attention has been given to intermediate hydrogen bonds. The experimental electron density distribution of α-deuterooxalic acid dihydrate has been previously determined at room temperature (Coppens, Sabine, Delaplane & Ibers, 1969). The current high-resolution study at 100 K provides significantly more detail in the density distribution allowing quantitative comparison with theoretical calculations (Stevens, 1980), and investigation of an intermediate hydrogen bond (2·5 Å) between the oxalic acid and water molecules, and the perturbation of the molecular density of the water by hydrogen bonding.

Experimental section

X-ray data collection and reduction

Crystals of α-oxalic acid dihydrate were obtained by slow evaporation of an aqueous solution. A long needle with cross-sectional dimensions of 0·41, 0·27 and 0·42 mm for the {101}, {10$\bar{1}$}, and {001} forms was cut to a length of 0·52 mm along the b axis. The crystal was attached to a glass fiber with silicone high-vacuum grease, mounted in an arbitrary orientation on a Picker FACS-1 automatic diffractometer, and cooled to 100 ± 5 K with a stream of cold nitrogen gas generated with a locally modified Enraf–Nonius universal low-temperature device. During data collection the gas-stream temperature was maintained within ±1 K as monitored with a copper–constantan thermocouple.

Table 1. *Crystal data for oxalic acid at* 100 K

The lattice dimensions were calculated from refinement of optimized setting angles of 20 reflections and λ(Mo $K\alpha_1$) = 0·70930 Å.

Space group	$P2_1/n$
a	6·0968 (7) Å
b	3·4975 (4)
c	11·9462 (15)
β	105·78 (1)°
V	245·12 Å^3
Z	2
D_x	1·708 Mg m^{-3}
μ(Mo $K\alpha$)*	0·170 mm^{-1}
M_r($C_2H_2O_4.2H_2O$)	126·07

* Based on mass absorption coefficients from *International Tables for X-ray Crystallography* (1974).

Unit-cell dimensions were obtained by least-squares refinement of the observed setting angles for the $K\alpha_1$ peaks of 20 centered reflections with $2\theta > 70°$. Scans of several systematically absent reflections confirmed the space group as $P2_1/n$. Crystal data for α-oxalic acid dihydrate are summarized in Table 1.

Intensity measurements were collected with Nb-filtered Mo $K\alpha$ radiation using a θ:2θ step-scan technique. Each reflection was scanned $2\theta(K\alpha_1) - 0.75°$ to $2\theta(K\alpha_2) + 0.75°$ using a step size of 0·03° in 2θ and a count time of 2 s/step. The full step-scan profile of each reflection was recorded on magnetic tape and analyzed to give the integrated intensity and its standard deviation (Blessing, Coppens & Becker, 1974). A total of 3979 reflections were collected in the hemisphere to $\sin\theta/\lambda = 0.90$ Å^{-1}.

Since a large proportion of the reflections above 0·90 Å^{-1} are weak, parameters from a preliminary least-squares refinement were used to predict the intensities of high-order reflections. Only reflections with intensities predicted to be greater than three times their estimated standard deviations were measured in the range $0.90 < \sin\theta/\lambda < 1.20$ Å^{-1}, yielding an additional 600 measurements.

Nine standard reflections measured after every 100 reflections showed a gradual decrease in intensity of 7% during data collection. Corrections to the intensity measurements were calculated from the behavior of the standards according to the procedure of McCandlish, Stout & Andrews (1975). A very strong reflection, $20\bar{4}$, included among the standards showed behavior similar to the other standards, indicating no change in extinction effects during data collection.

Previous room-temperature studies of oxalic acid encountered considerable anisotropy in the extinction (Delaplane & Ibers, 1969; Coppens & Sabine, 1969). In order to separate anisotropic extinction from other systematic effects, a second data set was collected with the same crystal in another orientation. The crystal was warmed to room temperature and remounted after rotation by approximately 90° about an axis perpendicular to the φ axis. A total of 6113 reflections were measured in a hemisphere up to $\sin\theta/\lambda = 1.08$ Å^{-1}. A decline of 4% in the intensities of the standards was observed during data collection. Data were processed in the same manner as the first set.

Absorption corrections were calculated by Gaussian numerical integration (Coppens, Leiserowitz & Rabinovich, 1965). Joint least-squares refinement of both data sets was used to determine a scale factor relating the two sets. Comparison of observed and calculated structure factors of the strongest reflections revealed only moderate extinction and no indication of anisotropy. The data from both sets were then merged and symmetry-related forms averaged to give a final set of 2315 independent reflections with internal agreement factors of $R(F^2) = 2.4\%$ and $R_w(F^2) = 4.1\%$. For the 3520 strongest reflections [$F^2 > 100\sigma(F^2)$], the agreement factors were $R(F^2) = 2.2$ and $R_w(F^2) = 1.8\%$.

Least-squares refinements

The quantity $\sum w(F_o - k|F_c|)^2$ with $w = 1/\sigma^2(F)$ was minimized by full-matrix least-squares refinement. The estimated standard deviation of each observation, $\sigma(F^2)$, was taken as the larger of σ_1 and σ_2, where $\sigma_1^2 = \sigma_{\text{count}}^2 + (0.02F^2)^2$ and $\sigma_2^2 = \sum_n (F_1^2 - \langle F^2\rangle)^2/(n-1)$ for n measurements of symmetry-related reflections. Reflections with both f_o and F_c less than $3\sigma(F)$ were considered 'unobserved' and were not included in the refinements.*

Atomic core, valence and total scattering factors for carbon and oxygen were taken from *International Tables for X-ray Crystallography* (1974). Hydrogen scattering factors used in the refinement were taken from Stewart, Davidson & Simpson (1965). The anomalous scattering factors of Cromer & Liberman (1970) were used for carbon and oxygen. Conventional refinement included adjustment of an overall scale factor, positional and anisotropic (except hydrogen) thermal parameters, and an isotropic secondary-extinction parameter. The best fit to observed intensities was obtained using an isotropic type I extinction model with a Lorentzian mosaic distribution (Becker & Coppens, 1974).

To reduce bias in refined parameters from the aspherical features of the valence electron density distribution, several refinements were made using only high-angle data for which the scattering is largely due to the core electrons. Comparison with results obtained from neutron diffraction measurements (Feld & Lehmann, 1979) indicated that bias in the oxygen positional parameters persists to high $\sin\theta/\lambda$ values requiring a lower limit of $\sin\theta/\lambda = 1.0$ Å^{-1} for data in the high-order refinements. Hydrogen contributes very little to scattering at high angles, and attempts to determine hydrogen positions from the high-order X-ray data were unsuccessful. Hydrogen atoms were therefore fixed at the positions determined by neutron diffraction. Comparison of the carbon and oxygen thermal parameters with those determined by neutron diffraction revealed a systematic difference, with the X-ray values about 20% higher.† Therefore, parameters from the high-order X-ray refinement rather than neutron values were used to calculate the electron

* A list of structure factors has been deposited with the British Library Lending Division as Supplementary Publication No. SUP 35154 (14 pp.). Copies may be obtained through The Executive Secretary, International Union of Crystallography, 5 Abbey Square, Chester CH1 2HU, England.

† A neutron data set collected very recently at Brookhaven is in better agreement with our X-ray data (McMullen & Koetzle, 1979).

density maps. Thermal parameters for hydrogen were calculated by multiplying the neutron values by the average ratio of the X-ray to neutron thermal parameters of oxygen and carbon.

An alternative technique for avoiding bias in the refined parameters is to include additional parameters in the least-squares refinement which describe the aspherical features of the valence density (Hansen & Coppens, 1978; Stewart, 1976; Harel & Hirshfeld, 1975). In this model deformations of the electron density at each atom are described by an expansion of multipole density functions,

$$\rho(\mathbf{r}) = \sum_{\text{atoms}} [\rho_{\text{core}}(\mathbf{r}) + P_v \rho_{\text{valence}}(\kappa' \mathbf{r}) + \sum_{l=0}^{4} R_l(\kappa'' r) \sum_{m=-l}^{l} P_{lm} y_{lm}(\mathbf{r}/r)],$$

where ρ_{core} and ρ_{valence} are spherical Hartree–Fock core and valence densities and the y_{lm} are spherical harmonic functions in real form. The radial functions $R_{lm}(r)$ are given by

$$R_l(r) = \frac{\zeta^{(n+3)}}{(n_l + 2)!} r^n l \exp(-\zeta_l r),$$

where n_l and ζ_l are chosen for each l according to Hansen & Coppens (1978). The P_v, P_{lm}, κ' and κ'' are refinable parameters. Positional and thermal parameters for the hydrogens have been fixed in the same manner as in the high-order refinements.

Electron density maps

Distortions of the atomic electron distributions in a molecule as a result of chemical bonding are revealed in a plot of the deformation density, $\Delta\rho$, defined as the difference between the total observed density and the density calculated for a superposition of spherical, neutral, Hartree–Fock atoms (the 'promolecule'). Positions and thermal parameters used in calculating the promolecule density have been taken from the high-order refinement except for the hydrogen atom for which values derived from neutron diffraction were used. Deformation maps have been calculated using the full X-ray data to a resolution of $\sin\theta/\lambda = 1{\cdot}20$ Å^{-1} corrected for extinction and anomalous dispersion. The scale factor was obtained by a cycle of refinement on k including the full data set with all other parameters fixed at the high-order values.

To provide a better three-dimensional description of the lone-pair density features around the oxygen atoms, the electron density distribution has been calculated on the surface of a sphere with radius 0·3 Å surrounding each oxygen and plotted in stereographic projection. Calculation of the density in stereographic projection is described by Stevens & Coppens (1977).

Since the contribution of experimental errors to the uncertainty in the experimental density varies with position (Rees, 1976), an estimate of the distribution of errors is required to make quantitative interpretations of features in the deformation density. Maps of the estimated standard deviations, $\sigma(\Delta\rho)$, have been calculated as described previously (Stevens, 1978).

Model deformation densities corresponding to the multipole refinement parameters have been calculated from the model structure factors and thus include thermal smearing and series-termination effects. If the multipole model is sufficiently flexible to fit the molecular density distribution, yet not flexible enough to accommodate random errors, then a result of the multipole refinement is to filter noise out of the experimental density. A final difference map, the residual density, has been calculated after the last cycle of the multipole refinement. The residual density is useful in judging the success of the model in fitting the significant features of the experimental density distribution.

Derived properties

Once the electron density distribution has been determined, other one-electron properties of the system may be derived either by a direct-space integration of $\rho(\mathbf{r})$ (Coppens & Guru Row, 1978) or by refinement of the structure factors with a model including analytical functions which describe the density features and subsequent calculation of the properties from the analytical functions (Hansen & Coppens, 1978; Coppens, Guru Row, Leung, Stevens, Becker & Yang, 1979).

In this study, molecular dipole moments and net molecular charges have been calculated by direct-space integration using the program *DEBYE* (Coppens & Hansen, 1977). Net molecular charges and molecular dipole moments have been calculated from refined multipole density functions using the program *MOLLY* (Hansen & Coppens, 1978).

Results and discussion

Refinement results

Results of various least-squares refinements are summarized in Table 2. Positional and thermal parameters from conventional refinement of the full data set (refinement I), from refinement of high-order data only (refinement II), and refinement including multipole density functions (refinement III) are given in Tables 3 and 4. Populations of the multipole density functions are listed in Table 5.

As expected, hydrogen positions determined from conventional refinement of the X-ray data show large shifts due to the aspherical distribution of electron

Table 2. *Summary of least-squares refinements*

Refinement	I	II	III
sin θ/λ range (Å^{-1})	0·0–1·2	1·0–1·2	0·0–1·2
N_{obs}	2108	463	2117
N_v	50	36	116
Scale factor	5·95 (1)	5·85 (6)	6·01 (1)
R factors			
R (%)	2·64	3·21	1·40
R_w (%)	3·79	1·94	1·61
R factors including rejected reflections			
R (%)	3·13	5·52	1·87
R_w (%)	3·81	2·04	1·66
GOF	2·53	1·38	1·10
Extinction (g_{iso})	$3·5(18)\times10^{-6}$	$[3·5\times10^{-6}]$	$14·3(9)\times10^{-6}$

Table 3. *Atomic coordinates*

Refinement I

	x	*y*	*z*
C(1)	−0·04507 (4)	0·05869 (8)	0·05196 (2)
O(1)	0·08539 (4)	−0·05636 (8)	0·15013 (2)
O(2)	−0·22146 (4)	0·24248 (7)	0·03627 (2)
O(3)	−0·45139 (4)	0·63112 (8)	0·17877 (2)
H(1)	0·0332 (17)	0·0299 (29)	0·2137 (8)
H(2)	−0·5659 (15)	0·6806 (27)	0·1159 (8)
H(3)	−0·3714 (14)	0·4731 (26)	0·1563 (7)

Refinement II

	x	*y*	*z*
C(1)	−0·04501 (9)	0·05885 (14)	0·05199 (3)
O(1)	0·08493 (10)	−0·05588 (18)	0·15004 (3)
O(2)	−0·22128 (9)	0·24233 (15)	0·03623 (3)
O(3)	−0·45153 (9)	0·63076 (16)	0·17862 (3)
H(1)	0·02339	0·02171	0·22280
H(2)	−0·57832	0·69677	0·11269
H(3)	−0·35811	0·45457	0·14954

Refinement III

	x	*y*	*z*
C(1)	−0·04484 (2)	0·05857 (4)	0·05196 (1)
O(1)	0·08511 (3)	−0·05617 (4)	0·15009 (2)
O(2)	−0·22142 (3)	0·24236 (4)	0·03626 (1)
O(3)	−0·45145 (2)	0·63088 (4)	0·17867 (1)
H(1)			
H(2)		(same as refinement II)	
H(3)			

density in the O—H bonds. Of the heavy atoms the largest asphericity shift is only 0·003 (1) Å for O(1) away from the C—O bond. The small asphericity shifts observed can be attributed to the generally symmetrical valence features surrounding each heavy atom and the large proportion of high-order reflections in the data set.

Positional parameters for carbon and oxygen atoms obtained from the high-order refinement agree with the neutron diffraction values of Feld & Lehmann (1979) within 0·001 Å except for the *y* coordinate of O(3) which differs by 0·002 Å. The systematic difference between high-order and neutron thermal parameters prevents a detailed comparison. However, after scaling

Table 4. *Atomic thermal parameters* (Å^2)

Refinement I

	U_{11}	U_{22}	U_{33}	U_{12}	U_{13}	U_{23}
C(1)	1030 (9)	1188 (10)	820 (8)	131 (7)	277 (6)	−2 (6)
O(1)	1376 (9)	2039 (11)	753 (6)	526 (7)	221 (6)	84 (6)
O(2)	1267 (9)	1874 (10)	1031 (7)	566 (7)	382 (6)	58 (6)
O(3)	1230 (8)	1977 (11)	927 (7)	332 (7)	374 (6)	121 (6)
H(1)	4740 (243)					
H(2)	3670 (184)					
H(3)	3107 (171)					

Refinement II

	U_{11}	U_{22}	U_{33}	U_{12}	U_{13}	U_{23}
C(1)	993 (12)	1164 (10)	759 (6)	180 (10)	261 (7)	−2 (8)
O(1)	1329 (13)	1960 (13)	717 (5)	506 (11)	217 (6)	68 (8)
O(2)	1254 (14)	1896 (12)	931 (6)	605 (11)	366 (8)	64 (8)
O(3)	1231 (13)	1907 (13)	869 (6)	299 (11)	382 (7)	108 (7)
H(1)	2709	3507	2190	363	634	10
H(2)	2860	4489	2499	810	19	639
H(3)	3261	4259	3730	1242	1560	−299

Refinement III

	U_{11}	U_{22}	U_{33}	U_{12}	U_{13}	U_{23}
C(1)	1028 (6)	1250 (6)	821 (5)	209 (4)	263 (3)	17 (3)
O(1)	1385 (5)	2037 (6)	785 (5)	531 (5)	233 (4)	76 (3)
O(2)	1289 (5)	1928 (6)	1002 (5)	597 (5)	378 (3)	66 (3)
O(3)	1271 (5)	1974 (6)	949 (4)	291 (4)	493 (3)	110 (3)
H(1)						
H(2)			(same as refinement II)			
H(3)						

Table 5. *Multipole populations*

Multipole parameters are defined with respect to local orthogonal coordinate systems centered on each atom (Fig. 2*b*).

Mirror-plane symmetry in the plane of the oxalic acid molecule and in the bisecting plane perpendicular to the plane of the water molecule has been imposed on the deformation parameters.

	C(1)	O(1)	O(2)	O(3)
κ'	0·975 (4)	0·990 (2)	0·990 (2)	0·990 (3)
κ''	0·79 (1)	1·19 (4)	1·00 (4)	1·01 (4)
P_v	4·30 (4)	6·12 (3)	6·08 (3)	6·11 (5)
P_{11+}	0·088 (10)	−0·048 (5)	−0·071 (8)	−0·077 (10)
P_{11-}	0·011 (7)	−0·035 (5)	0·006 (5)	0·015 (5)
P_{20}	−0·266 (10)	−0·007 (6)	−0·062 (7)	−0·058 (6)
P_{22+}	−0·032 (7)	0·019 (5)	0·005 (5)	0·015 (5)
P_{22-}	0·096 (8)	−0·034 (5)	−0·061 (6)	−0·026 (5)
P_{31+}	0·006 (7)	0·020 (4)	0·010 (5)	0·068 (6)
P_{31-}	−0·025 (6)	−0·023 (4)	−0·014 (4)	−0·021 (4)
P_{33+}	0·340 (16)	0·061 (4)	0·036 (5)	0·000 (4)
P_{33-}	−0·032 (7)	0·009 (3)	0·003 (4)	−0·005 (4)
P_{40}	0·038 (9)	0·013 (5)	−0·001 (6)	0·002 (6)
P_{42+}	−0·007 (9)	−0·003 (5)	−0·009 (6)	0·044 (7)
P_{42-}	−0·014 (7)	−0·015 (5)	−0·009 (6)	−0·011 (5)
P_{44+}	−0·021 (9)	0·022 (4)	−0·016 (6)	0·006 (5)
P_{44-}	0·001 (8)	0·010 (4)	−0·004 (5)	0·010 (5)

	H(1)	H(2)	H(3)*
κ'	1·09 (2)	1·22 (2)	1·22
κ''	1·05 (7)	0·85 (3)	0·85
P_v	0·77 (3)	0·81 (3)	0·81
P_{10}	0·070 (7)	0·176 (14)	0·176
P_{20}	0·087 (11)	0·099 (12)	0·099

* H(3) populations are constrained equal to H(2).

the neutron thermal parameters by the average ratio $(U_{ii,X}/U_{ii,N})$ for the heavy atoms, the root-mean-square value of $\Delta U_{ii}/(\sigma_X^2 + \sigma_N^2)^{1/2}$ is only 1·14, indicating good agreement except for an overall scale difference, which may be due to a mismatch in temperatures.

Interatomic distances and angles from conventional and high-order refinements are compared in Table 6 with neutron diffraction values at 100 K (Feld & Lehmann, 1979) and room temperature (Sabine, Cox & Craven, 1969). Estimated standard deviations in distances and angles are calculated using the full least-squares variance–covariance matrix, except with neutron values where standard errors are used. The agreement between high-order X-ray and neutron bond distances and angles is remarkably good.

Comparison with room-temperature intermolecular distances reveals that O···O distances along the normal hydrogen bonds are reduced by 0·045 Å on cooling to 100 K. The short hydrogen-bond O···O distance is reduced by 0·02 Å while the O(1)—H(1) bonded distance increases from 1·026 (7) to 1·071 (1) Å. The shift of the hydrogen atom toward the center of the strong hydrogen bond is in agreement with the well known correlation between O—H and O···O distances (Hamilton & Ibers, 1968). The geometry of this hydrogen bond is clearly intermediate between the shortest symmetrical hydrogen bonds and normal hydrogen bonds.

Electron density maps

The experimental deformation density calculated in the plane of the oxalic acid molecule is shown in Fig. 1. As expected, peaks are found between all covalently bonded atoms and in the lone-pair regions of oxygen atoms. All of the density features are higher and more clearly defined compared with the previous study (Coppens, Sabine, Delaplane & Ibers, 1969), due to the higher resolution and lower temperature of the present study.

The estimated distribution of errors in the deformation density for the section through the oxalic acid molecule is also plotted in Fig. 1. The estimated $\sigma(\Delta\rho)$ is 0·02 e/Å^3 except near the center of symmetry (0·03 e/Å^3) and near the atomic centers where the error rapidly increases to over 0·9 e/Å^3 at positions of the O and C atoms. The effects of series termination on the features of the deformation are shown in the graph of peak heights *vs* resolution limit (Fig. 2). As observed in other low-temperature studies (Wang, Blessing, Ross & Coppens, 1976; Stevens, 1978), sharper features of the density distribution such as the lone-pair peaks are the most affected by series termination. Plots of the density distribution calculated using only low-order data contain less experimental noise, but fail to reproduce quantitatively the lone-pair peak heights (Stevens, 1977, 1978).

Table 6. *Bond lengths* (Å) *and angles* (°) *for α-oxalic acid dihydrate*

	Full data[a] 100 K	High-order[a,b] 100 K	Neutron[c] 100 K	Neutron[d] room temperature
C(1)–C(1′)	1·544 (1)	1·544 (1)	1·544 (1)	1·536 (3)
C(1)–O(1)	1·289 (1)	1·287 (1)	1·287 (1)	1·291 (5)
C(1)–O(2)	1·223 (1)	1·222 (1)	1·222 (1)	1·212 (4)
O(1)–H(1)	0·949 (16)	1·071 (1)	1·071 (1)	1·026 (7)
O(3)–H(2)	0·892 (15)	0·970 (1)	0·969 (1)	0·964 (7)
O(3)–H(3)	0·828 (14)	0·966 (1)	0·967 (1)	0·956 (9)
H(1)···O(3′)	1·540 (15)	1·416 (1)	1·417 (1)	1·480 (7)
H(2)···O(2″)	1·943 (15)	1·876 (1)	1·877 (1)	1·917 (8)
H(3)···O(2)	2·063 (13)	1·922 (1)	1·921 (1)	1·979 (9)
O(1)···O(3′)	2·487 (1)	2·487 (1)	2·487 (1)	2·506 (4)
O(3)···O(2″)	2·826 (1)	2·825 (1)	2·825 (1)	2·864 (5)
O(3)···O(2)	2·830 (1)	2·830 (1)	2·830 (1)	2·881 (4)
O(1)–C(1)–O(2)	127·07 (2)	127·02 (5)	126·98 (3)	126·6 (3)
O(1)–C(1)–C(1′)	112·45 (3)	112·56 (7)	112·59 (3)	112·4 (3)
O(2)–C(1)–C(1′)	120·48 (3)	120·41 (5)	120·43 (3)	121·0 (3)
C(1)–O(1)–H(1)	111·7 (9)	113·3 (1)	113·3 (1)	114·4 (6)
H(2)–O(3)–H(3)	104·6 (12)	106·1 (2)	106·1 (2)	105·9 (7)
O(1)–H(1)···O(3′)	174·6 (16)	177·5 (1)	177·5 (1)	179·3 (6)
H(1)···O(3′)–H(2′)	112·9 (11)	112·4 (2)	112·3 (1)	112·8 (7)
H(1)···O(3′)–H(3′)	118·0 (11)	118·3 (2)	118·1 (1)	116·8 (4)
O(3)–H(2)···O(2″)	169·9 (13)	165·2 (1)	165·2 (1)	166·9 (6)
H(2)···O(2″)–C(1″)	123·5 (4)	121·6 (2)	121·6 (1)	122·8 (6)
O(3)–H(3)···O(2)	153·8 (13)	155·7 (2)	155·6 (1)	156·6 (7)
H(3)···O(2)–C(1)	129·5 (4)	128·8 (2)	128·8 (1)	129·5 (7)

(*a*) This investigation. (*b*) Hydrogen position from Feld & Lehmann (1979). (*c*) Feld & Lehmann (1979). (*d*) Sabine, Cox & Craven (1969).

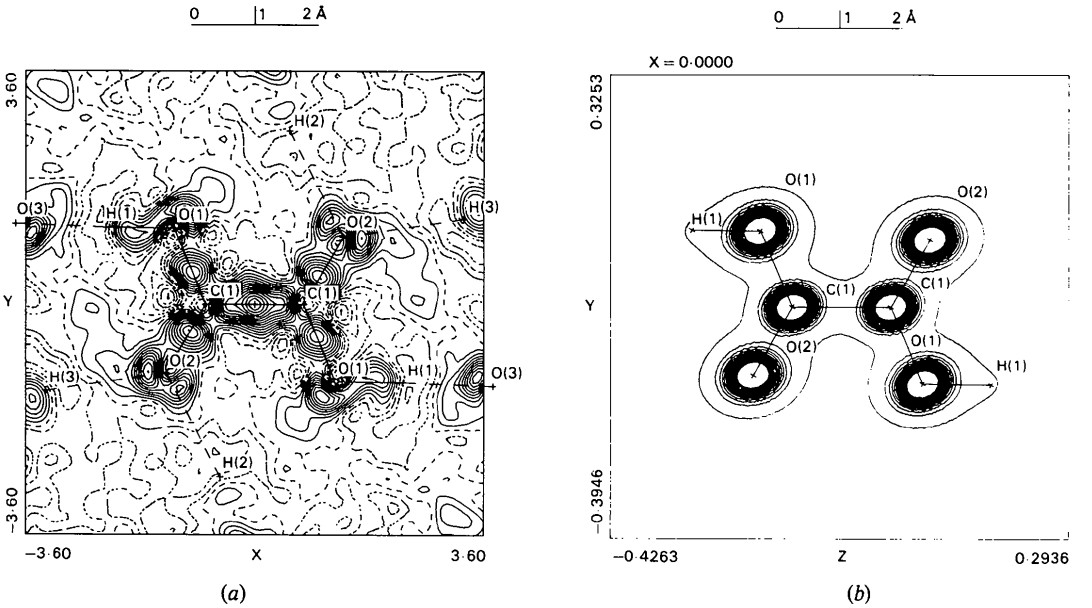

Fig. 1. (*a*) Experimental deformation density in the plane of the oxalic acid molecule. Contours are at 0·05 e/Å^3 intervals with the zero and negative contours dashed. (*b*) Estimated error distribution of the deformation density in the oxalic acid molecular plane. Contours at 0·02 e/Å^3 intervals, lowest contour plotted at 0·04 e/Å^3.

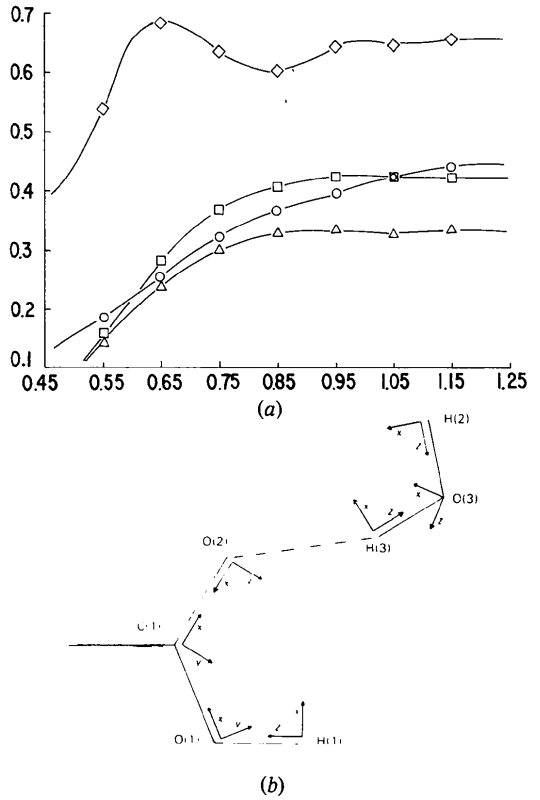

Fig. 2. (*a*) Bond and lone-pair peak heights plotted as a function of experimental resolution limit. ◇ C—C bond; □ average of C—O bonds; △ average of O—H bond; ○ average of lone-pair peaks. (*b*) Local atomic coordinate systems used in the multipole refinement.

An interesting feature of the electron density distribution in the oxalic acid molecule is the large peak in the C—C bond. The elongation of the peak is similar to that observed in several other high-resolution studies (see for example Stevens, 1978; Kvick, Koetzle & Stevens, 1979; Hansen & Coppens, 1978). Although the bond is rather long [1·554 (1) Å] for a C—C bond, it contains considerable π character as shown in sections perpendicular to the bond axis (Fig. 3). Sections through the C—O and C=O bonds are also shown in Fig. 3. Significant π character of the C—C bond was observed in $NaHC_2O_4.H_2O$ (Tellgren, Thomas & Olovsson, 1977) and was also noted in the C—O and C=O bonds of oxalic acid (Coppens, Sabine, Delaplane & Ibers, 1969) and in theoretical densities of the oxalic acid molecule (Johansen, 1979; Stevens, 1980).

To investigate further the deviations of these bond peaks from cylindrical symmetry, the cylindrical component has been removed by calculating the double difference density, $\rho_{L\neq 0} = \Delta\rho - \Delta\rho(90°)$, where $\Delta\rho(90°)$ is the deformation density perpendicular to the bond axis and rotated 90° around the bond center. In addition, *mm* symmetry has been imposed on the planes by averaging. Thus, only the π-bonding $p_\pi p_\pi$ (or higher-symmetry) orbital products contribute to $\rho_{L\neq 0}$. Plots of $\rho_{L\neq 0}$ for the C—C, C—O and C=O bonds are given in Fig. 4.

The C—C bond shows the largest deviation from cylindrical symmetry with a difference of $\rho_{L\neq 0}$ = 0·23 (2) e/Å^3 at 0·45 Å above and below the molecular

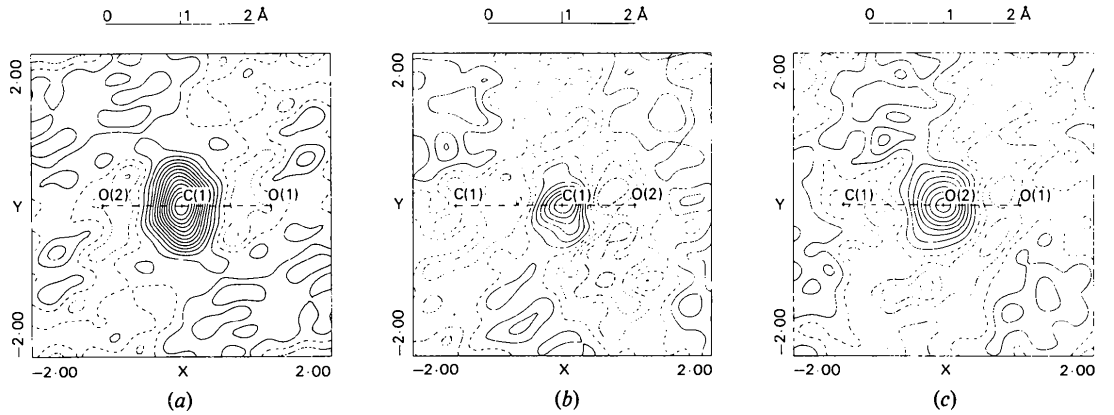

Fig. 3. Sections of the deformation density perpendicular to the bond axes at the bond midpoints. Contours as in Fig. 1(*a*). (*a*) C–C bond; (*b*) C–O(1) bond; (*c*) C–O(2) bond.

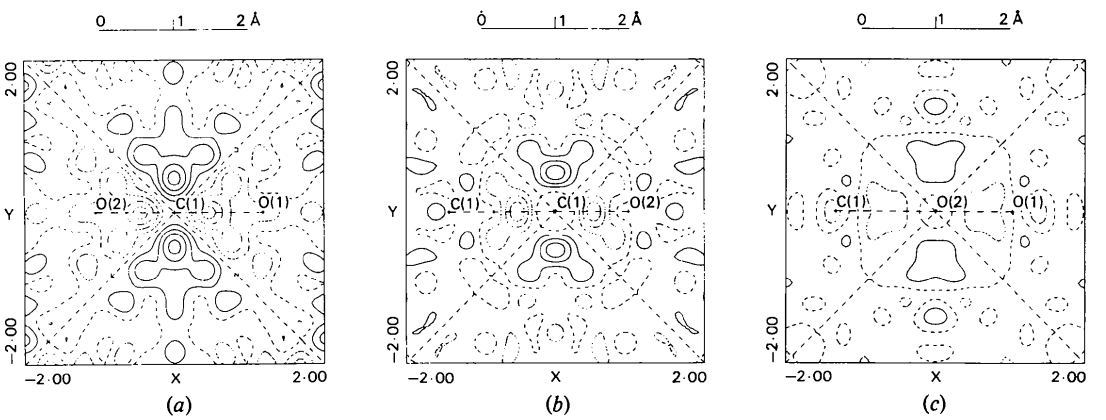

Fig. 4. Plots of the difference between sections perpendicular to the molecular plane and the same plane rotated by 90° about the bond axis. Contours as in Fig. 1(*a*). (*a*) C–C bond; (*b*) C–O(1) bond; (*c*) C–O(2) bond.

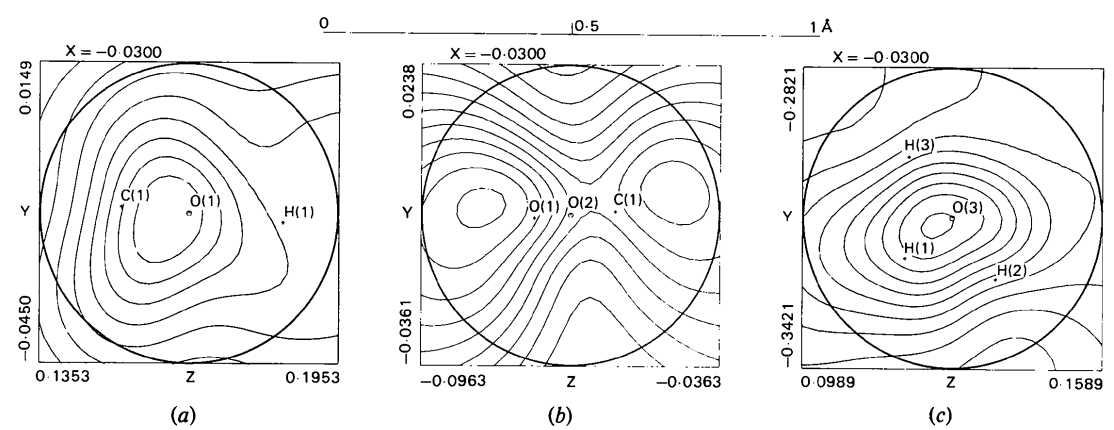

Fig. 5. Stereographic projection of the deformation density on the surface of a sphere with 0·3 Å radius centered at the oxygen atom. Contours as in Fig. 1(*a*). (*a*) Projection of the 'outward' hemisphere centered on O(1) onto a plane perpendicular to the line bisecting the H–O–C angle. (*b*) Projection of the hemisphere centered on O(2) and opposite the C=O bond onto a plane perpendicular to the bond. (*c*) Projection of the 'outward' hemisphere centered on O(3) onto a plane perpendicular to the line bisecting the H–O–H angle.

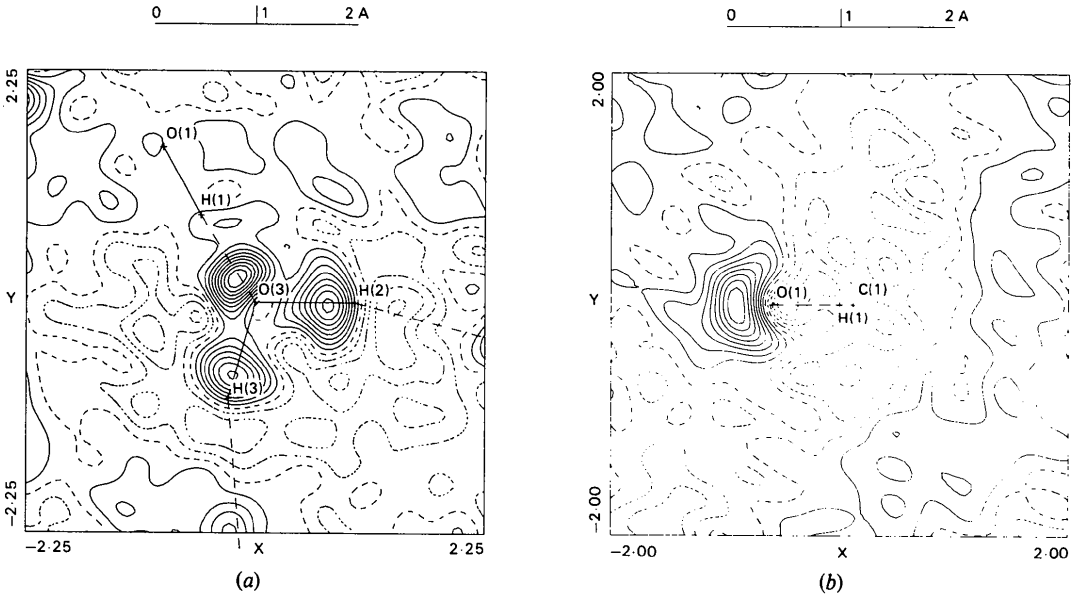

Fig. 6. (*a*) Experimental deformation density plotted in the plane of the water molecule. Contours as in Fig. 1(*a*). (*b*) Section of the deformation density perpendicular to the oxalic acid plane through O(1) and bisecting the C—O—H angle. Contours as in Fig. 1(*a*).

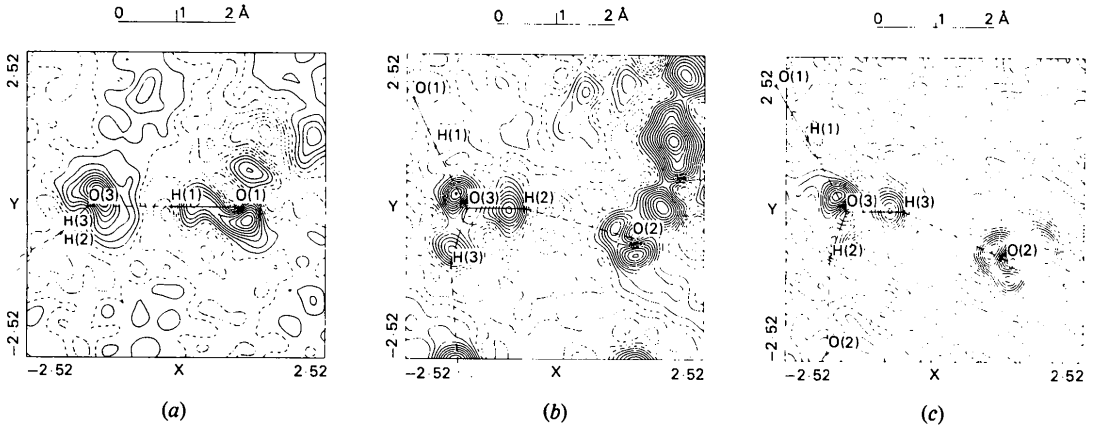

Fig. 7. Sections of the deformation density containing the hydrogen bonds. Contours as in Fig. 1(*a*). (*a*) Section perpendicular to the plane of the water molecule and containing the O(3′)···H(1) short hydrogen bond. (*b*) Plane defined by the positions of O(3), H(2) and O(2″). (*c*) Plane defined by the positions of O(3), H(3) and O(2).

plane. Despite the difference in bond lengths, the formally single C(1)—O(1) bond shows a larger $\rho_{L\neq 0}$ difference [0·19 (2) e/Å^3] than the formally double C(1)—O(2) bond [0·07 (2) e/Å^3]. Although thermal motion is larger perpendicular to the molecular plane, the difference in r.m.s. amplitudes contributes little to the observed elongation perpendicular to the plane because of the fairly diffuse nature of the valence density.

Stereographic projections of the deformation density in the lone-pair regions of the oxygen atoms are shown in Fig. 5. In the molecular plane, two maxima of non-bonding density are revealed in the projection about O(2). This distribution is consistent with the expected sp^2 hybridization at O(2). The stereographic projection about O(1) shows only a single peak in the molecular plane suggesting an sp^2-hybridized lone pair in addition to the two covalent bonds to this atom.

The section of the deformation density in the plane of the water molecule is plotted in Fig. 6(*a*). The quality of the water molecule deformation density is evident in the two nearly equal [0·36 (2) and 0·42 (2) e/Å^3] O—H bond peaks and the distinct lone-pair peak at the back of the oxygen atom. These features may be compared with previous experimental deformation densities for crystalline hydrates (Coppens, Sabine, Delaplane &

Ibers, 1969; Taylor & Sabine, 1972; Bats, 1977; Tellgren, Thomas & Olovsson, 1977; Thomas, 1978; Olovsson, Kvick, Lehmann & Olovsson, 1980). Clearly, low-temperature measurements are essential to an accurate study of the electron distribution in the water molecule.

Stereographic projection of the non-bonding density around O(3) (Fig. 5*c*) reveals only a single peak elongated perpendicular to the plane of the water molecule. The two peaks expected in the deformation density for sp^3 hybridization of an isolated water molecule apparently are merged into a single peak by thermal smearing and limited experimental resolution. A single peak is therefore not in disagreement with theoretical densities of the water molecule (Smith, 1977; Stevens, 1980).

The plane perpendicular to the water molecule containing the short hydrogen bond is plotted in Fig. 7. A striking feature of the lone-pair peak is the polarization of the density toward the side of the molecule which accepts the short hydrogen bond. The asymmetry of the lone-pair density is also evident in the stereographic projection (Fig. 5*c*). The distortion of the non-bonding density from mirror-plane symmetry is one of the clearest examples of perturbation of an experimental density distribution by hydrogen bonding. Recently, very similar distortions have been observed in two independent water molecules in the structure of *trans*-2,5-dimethylhexene-2,5-diol hemihydrate (van der Wal, 1979). An asymmetry in the lone-pair peak of the water molecule in lithium formate monohydrate was also observed by Thomas, Tellgren & Almlöf (1975) but uncertainties associated with a room-temperature study of a non-centrosymmetric structure prevented any definite conclusions.

Hydrogen bonds

A small charge deficiency in the deformation density is found between the donor and acceptor in each of the hydrogen bonds. The density distributions in the O(3)–H(2)···O(2) and O(3)–H(3)···O(2) hydrogen bonds are given in Fig. 7(*b*) and (*c*). Similar charge deficiencies have been observed in several accurate studies of OH···O and NH···O hydrogen bonds (for example Almlöf, Kvick & Thomas, 1973; Stevens, 1978; Takusagawa & Koetzle, 1979; Kvick, Koetzle & Stevens, 1979). Theoretical calculations of the electron density distribution (Dreyfus & Pullman, 1970; Yamabe & Morokuma, 1975) show that the charge deficiency is primarily due to the electrostatic contribution which is also the largest term in the bond energy.

A difference between the short and normal hydrogen bonds is apparent in maps of the deformation density in which the density of the hydrogen atom is not subtracted (Fig. 8). This modified function displays the valence density in the hydrogen-bonded region.* For the long hydrogen bonds, a clear break is present in the H(3)···O(2) region and only a slight positive peak in the H(2)···O(2) hydrogen bond (Fig. 8*b*, *c*). On the other hand, the short hydrogen bond shows a continuous ridge of density with a saddle point of 0·24 (3) e/Å^3 between the oxalic acid proton and the water oxygen atom. A continuous ridge of density 0·55 e/Å^3 high was observed in the short symmetrical hydrogen bond [O···O distance 2·452 (3) Å] of sodium hydrogen diacetate (Stevens, Lehmann & Coppens, 1977) and was interpreted as giving evidence for a larger covalent contribution to short hydrogen bonds. In sodium hydrogen maleate trihydrate a similar ridge with a saddle point of height 0·4 e/Å^3 is also found along the short (2·445 Å) intramolecular hydrogen bond (Olovsson, Kvick, Lehmann & Olovsson, 1980; Olovsson, 1980). Thus the valence density in the hydrogen bond in oxalic acid is intermediate between that found for short bonds and for long hydrogen

* True valence maps, in which only core densities are subtracted for carbon and oxygen, are essentially identical in the hydrogen-bond region, but suffer more from series-termination errors.

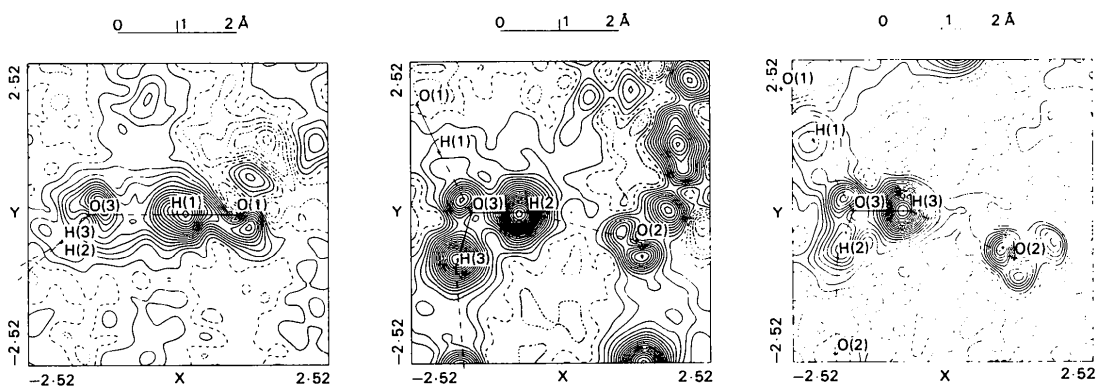

(*a*) (*b*) (*c*)

Fig. 8. Sections of the deformation calculated without subtracting the hydrogen-atom density. Contours as in Fig. 1(*a*). (*a*) Same plane as in Fig. 6(*a*). (*b*) Same plane as in Fig. 6(*b*). (*c*) Same plane as in Fig. 6(*c*).

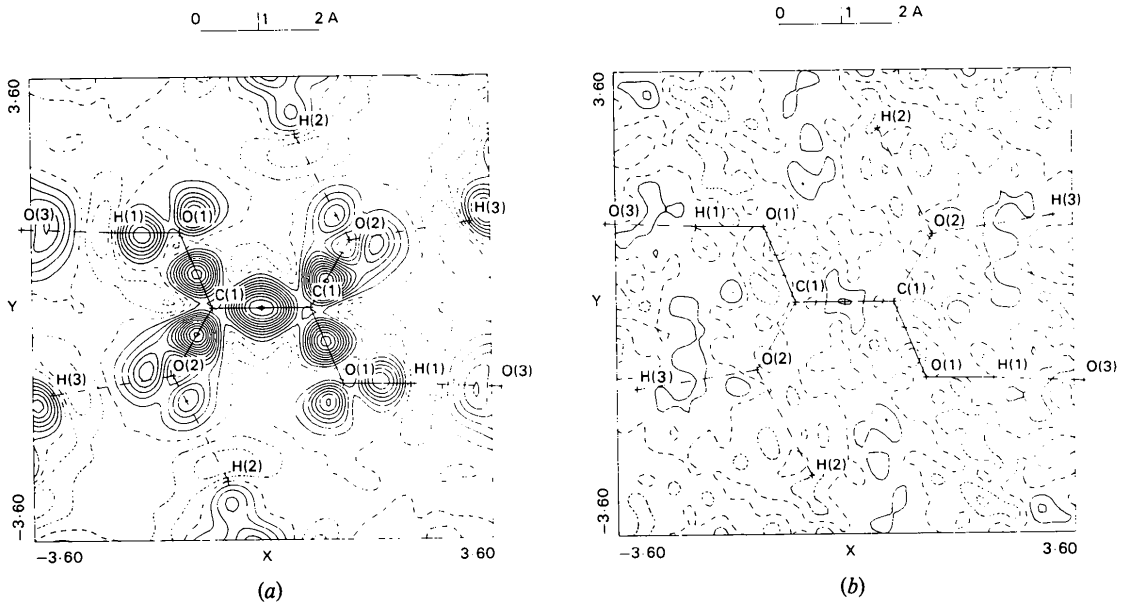

Fig. 9. (*a*) Multipole model density calculated in the plane of the oxalic acid molecule. (*b*) Residual density calculated in the molecular plane. Contours as in Fig. 1(*a*).

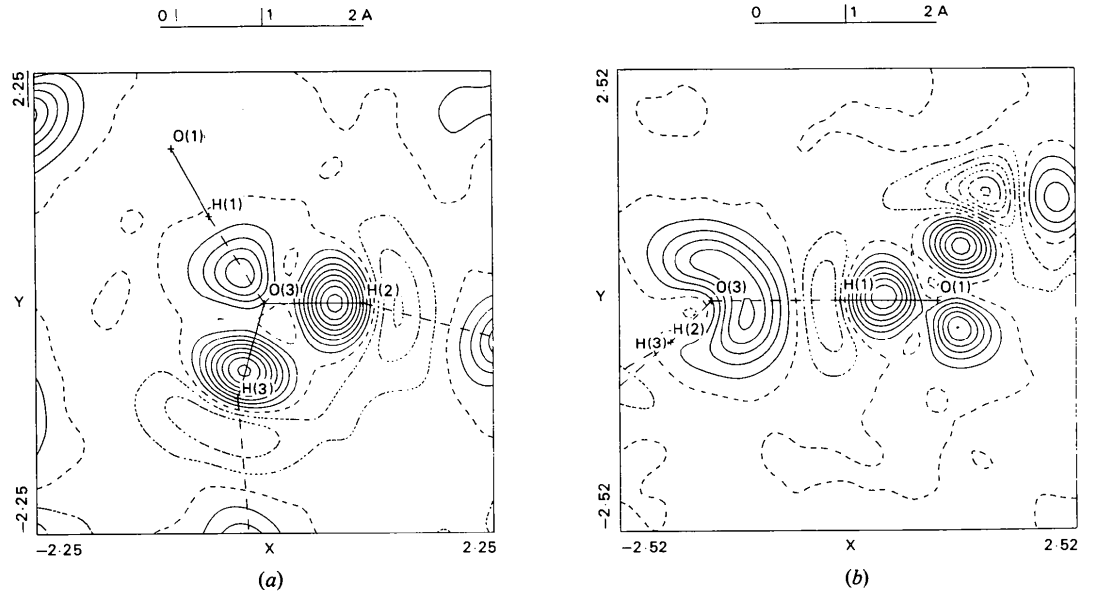

Fig. 10. (*a*) Model density calculated in the plane of the water molecule. (*b*) Model density in the plane perpendicular to the water molecule and containing the short hydrogen bond. Contours as in Fig. 1(*a*).

bonds. These results suggest that covalent contributions are not limited to the shortest bonds but decrease gradually as the hydrogen-bond length increases.

Multipole model and residual densities

The multipole model density in the plane of the oxalic acid molecule is plotted in Fig. 9 along with the corresponding residual density. Over most of the molecule the density is very similar to the experimental deformation density (Fig. 1*a*), although the peak shapes generally show less detail. The lone-pair peaks of all three oxygen atoms, however, are lower and more diffuse in the model density. The residual density does not show any systematic features at the lone-pair positions. The differences between the experimental and

model densities must therefore be absorbed by small changes in other parameters. For example, the temperature factors of refinement III are systematically higher than those of refinement II. The difficulty of the multipole functions in the lone-pair region may be due in part to the restricted radial form of the functions which must account for both the sharp lone-pair peaks and more diffuse bond peaks with only a single adjustable radial parameter for high multipoles.

Multipole model densities calculated in the plane of the water molecule and in the plane containing the short hydrogen bond are plotted in Fig. 10. Both model maps show essentially the same features as the experimental deformation density including the asymmetry of the lone-pair density on the water molecule.

Net charges and dipole moments

Direct integration of the deformation density of the water molecule within a polyhedral volume defined by planes perpendicular to the intermolecular vectors between atoms (Coppens & Hansen, 1977) gives a net charge of +0·16 (3) e on the water molecule and a dipole moment of 6·40 (17) × 10^{-30} Cm [1·92 (5) Debye]. The dipole-moment vector lies on the plane bisecting the H(2)—O(3)—H(3) angle but makes an angle of 35 (5)° with the plane of the water molecule.

The multipole population parameters (Table 5) yield a net charge on the water molecule of +0·27 (7) e and a dipole moment of 7·0 (7) × 10^{-30} Cm [2·1 (2) Debye] with a deviation of 15 (4)° from the molecular plane. The positive charge found on the water molecule is similar to charges of about +0·2 e found in other crystalline hydrates (Coppens, Pautler & Griffin, 1971; Bats, 1977).

The dipole moments calculated by both methods are slightly higher than the experimental value of 6·158 (17) × 10^{-30} Cm [1·846 (5) Debye] (Birnbaum & Chatterjie, 1952) for the isolated molecule. Similar results have been obtained for sulfamic acid and formamide (Coppens *et al.*, 1979) indicating that dipole moments may be increased by interactions with the molecular environment. In both cases the deviation of the dipole moment from the molecular plane is in the direction of the short hydrogen bond, in agreement with the observed asymmetry in the deformation density.

Conclusion

As pointed out by Coulson (1959), the hydrogen-bonding interaction must be described in terms of several components which may all play significant roles depending on O···O separation. In oxalic acid, a hydrogen bond of intermediate length is found to have an electron density distribution which is intermediate between the densities which have been observed in short and normal hydrogen bonds. Although a partitioning of the experimental density into various contributions [as has been done with theoretical hydrogen-bond densities by Yamabe & Morokuma (1975), for example] is not possible, a continuous change in electron distribution with increasing bond length suggests a gradual decrease in the covalent contribution from the case of the short hydrogen bond to the essentially electrostatic interaction of long bonds.

The clearly observable perturbation of the electron density indicates that the effects of intermolecular interaction in crystals will be observable in careful experimental studies. Also, the low level of experimental noise in the present maps will provide a stringent test for quantitative comparisons with theoretical calculations.

We wish to thank Drs R. Feld and M. S. Lehmann for permission to use their neutron results prior to publication. Support of this work by the National Science Foundation (CHE 76-13342 AO1) is gratefully acknowledged.

References

ALLEN, L. C. (1975). *J. Am. Chem. Soc.* **97**, 6921–6940.
ALMLÖF, J., KVICK, Å. & THOMAS, J. O. (1973). *J. Chem. Phys.* **59**, 3901–3906.
BATS, J. W. (1977). *Acta Cryst.* B**33**, 466–472.
BECKER, P. J. & COPPENS, P. (1974). *Acta Cryst.* A**30**, 129–147.
BIRNBAUM, G. & CHATTERJIE, S. K. (1952). *J. Appl. Phys.* **23**, 220–223.
BLESSING, R. H., COPPENS, P. & BECKER, P. (1974). *J. Appl. Cryst.* **7**, 488–492.
COPPENS, P. (1975). *MTP International Review of Science, Physical Chemistry, Series* 2, Vol. 11. London: Butterworths.
COPPENS, P. (1977). *Angew. Chem. Int. Ed. Engl.* **16**, 33–40.
COPPENS, P. & GURU ROW, T. N. (1978). *Ann. N.Y. Acad. Sci.* **313**, 214–255.
COPPENS, P., GURU ROW, T. N., LEUNG, P., STEVENS, E. D., BECKER, P. J. & YANG, Y. W. (1979). *Acta Cryst.* A**35**, 63–72.
COPPENS, P. & HANSEN, N. K. (1977). *Isr. J. Chem.* **16**, 163–167.
COPPENS, P., LEISEROWITZ, L. & RABINOVICH, D. (1965). *Acta Cryst.* **18**, 1035–1038.
COPPENS, P., PAUTLER, D. & GRIFFIN, J. F. (1971). *J. Am. Chem. Soc.* **93**, 1051–1058.
COPPENS, P. & SABINE, T. M. (1969). *Acta Cryst.* B**25**, 2445–2451.
COPPENS, P., SABINE, T. M., DELAPLANE, R. G. & IBERS, J. A. (1969). *Acta Cryst.* B**25**, 2451–2458.
COPPENS, P. & STEVENS, E. D. (1977). *Advances in Quantum Chemistry*, Vol. 10. New York: Academic Press.
COULSON, C. A. (1959). *Hydrogen Bonding*, edited by D. HADZI, pp. 339–360. London: Pergamon Press.

CROMER, D. T. & LIBERMAN, D. (1970). *J. Chem. Phys.* **53**, 1891–1898.
DELAPLANE, R. G. & IBERS, J. A. (1969). *Acta Cryst.* B**25**, 2423–2437.
DESMEULES, P. J. & ALLEN, L. C. (1980). To be published.
DREYFUS, M. & PULLMAN, A. (1970). *Theor. Chim. Acta*, **19**, 20–37.
FELD, R. & LEHMANN, M. S. (1979). Unpublished results.
GRIFFIN, J. F. & COPPENS, P. (1975). *J. Am. Chem. Soc.* **97**, 3496–3505.
HAMILTON, W. C. & IBERS, J. A. (1968). *Hydrogen Bonding in Solids*. New York: Benjamin.
HANSEN, N. K. & COPPENS, P. (1978). *Acta Cryst.* A**34**, 909–921.
HAREL, M. & HIRSHFELD, F. L. (1975). *Acta Cryst.* B**31**, 162–172.
International Tables for X-ray Crystallography (1974). Vol. IV. Birmingham: Kynoch Press.
JOHANSEN, H. (1979). *Acta Cryst.* A**35**, 319–325.
KOLLMAN, P. A. (1977). *Applications of Electron Structure Theory*, edited by H. F. SCHAEFER, pp. 109–152. New York: Plenum.
KOLLMAN, P. A. & ALLEN, L. C. (1972). *J. Am. Chem. Soc.* **94**, 6101–6107.
KVICK, Å., KOETZLE, T. F. & STEVENS, E. D. (1979). *J. Chem. Phys.* **71**, 173–179.
KVICK, Å., THOMAS, R. & KOETZLE, T. F. (1976). *Acta Cryst.* B**32**, 224–231.
MCCANDLISH, L. E., STOUT, G. H. & ANDREWS, L. C. (1975). *Acta Cryst.* A**31**, 245–249.
MCMULLEN, R. K. & KOETZLE, T. F. (1979). Private communication.
OLOVSSON, G., KVICK, Å., LEHMANN, M. & OLOVSSON, I. (1980). To be published.
OLOVSSON, I. (1980). *NATO Advanced Study Institute. Electronic & Magnetic Distributions in Molecules and Crystals*, edited by P. BECKER. New York: Plenum.
REES, B. (1976). *Acta Cryst.* A**32**, 483–488.
SABINE, T. M., COX, G. W. & CRAVEN, B. M. (1969). *Acta Cryst.* B**25**, 2437–2441.
SCHLEMPER, E. O. & HSU, B. (1978). *Am. Crystallogr. Assoc. Abstr.* **6**, 15.
SMITH, V. H. (1977). *Phys. Scr.* **15**, 147–162.
STEVENS, E. D. (1977). *Acta Cryst.* A**33**, 580–584.
STEVENS, E. D. (1978). *Acta Cryst.* B**34**, 544–551.
STEVENS, E. D. (1980). *Acta Cryst.* B**36**, 1876–1886.
STEVENS, E. D. & COPPENS, P. (1977). *J. Cryst. Mol. Struct.* **7**, 251–255.
STEVENS, E. D., LEHMANN, M. S. & COPPENS, P. (1977). *J. Am. Chem. Soc.* **99**, 2829–2831.
STEWART, R. F. (1976). *Acta Cryst.* A**32**, 565–574.
STEWART, R. F., DAVIDSON, E. R. & SIMPSON, W. T. (1965). *J. Chem. Phys.* **42**, 3175–3187.
TAKUSAGAWA, F. & KOETZLE, T. F. (1979). *Acta Cryst.* B**35**, 867–877.
TAYLOR, J. C. & SABINE, T. M. (1972). *Acta Cryst.* B**28**, 3340–3351.
TELLGREN, R., THOMAS, J. O. & OLOVSSON, I. (1977). *Acta Cryst.* B**33**, 3500–3504.
THOMAS, J. O. (1978). *Acta Cryst.* A**34**, 819–823.
THOMAS, J. O., TELLGREN, R. & ALMLÖF, J. (1975). *Acta Cryst.* B**31**, 1946–1955.
WAL, H. VAN DER (1979). Thesis, Univ. of Groningen, Groningen, The Netherlands.
WANG, Y., BLESSING, R. H., ROSS, F. K. & COPPENS, P. (1976). *Acta Cryst.* B**32**, 572–578.
YAMABE, S. & MOROKUMA, K. (1975). *J. Am. Chem. Soc.* **97**, 4458–4465.

Acta Cryst. (1980). B**36**, 1876–1886

Comparison of Theoretical and Experimental Electron Density Distributions of Oxalic Acid Dihydrate

BY E. D. STEVENS

Chemistry Department, State University of New York at Buffalo, Buffalo, New York 14214, *USA*

(*Received* 13 *August* 1979; *accepted* 24 *March* 1980)

Abstract

Thermally smeared theoretical electron density distributions of the oxalic acid molecule are compared with the experimental density of α-oxalic acid dihydrate obtained from high-resolution X-ray diffraction measurements at 100 K. Theoretical densities are calculated from extended-basis-set and 4-31G wavefunctions and smeared using experimental rigid-body translational and librational thermal parameters. Over much of the molecule, the agreement between the experimental and etended-basis-set theoretical density is within twice the estimated standard deviation of the experimental density. The largest significant differences are attributed to the effects of hydrogen bonding neglected in the theoretical calculations. The agreement between the experimental and dynamic 4-31G theoretical density is significantly worse. Comparison of static multipole model densities with static theoretical densities indicates that sharp features of the

0567-7408/80/081876-11$01.00